Contrails

TITAN III 20 PERCENT DYNAMIC MODEL CHARACTERISTICS – COMPARISON OF THEORY AND EXPERIMENT

George Morosow*
Ivan J. Jaszlics**
Martin Company, Denver Division, Colorado

Although the theory used to obtain dynamic characteristics of aerospace structures has been developed to a considerable extent, there are times when experimental verification is required, expecially when the structure is unconventional or extremely complex. This has been the case with Titan III. The vibration analyses of various Titan III configurations have been performed using the eigenvalue solution for a system of 80 degrees of freedom. This number of coordinates is required because the motion occurs in more than one direction simultaneously. The results of the analyses have been compared with the experimental data obtained from the vibration test of a 20 percent dynamically similar model at NASA, Langley Field, Hampton, Virginia. The comparison demonstrated a high degree of accuracy of the analytical results. It further demonstrated that model testing technique is, in most cases, an adequate substitute for full scale testing.

LIST OF MAJOR SYMBOLS

U	potential energy
T	kinetic energy
EI	bending modulus
kAG	shear modulus
k_{ij}	stiffness influence coefficient
δ_i	linear displacement
θ_i	angular displacement
η	local coordinate
V_i	applied shear
M_i	applied moment
l	bay length
$M(\eta)$	running mass
$I(\eta)$	running moment of inertia

*Head, Loads and Dynamics Unit
**Design Specialist, Loads and Dynamics Unit

PRECEDING PAGE BLANK

Approved for Public Release

Contrails

$\vec{r}$	position vector
$\xi(i)$	normal coordinate
ϕ	modal displacement
M_{eq}	generalized modal mass
$q(i)$	generalized coordinate

1. INTRODUCTION

Generally, there are two reasons why dynamic characteristics of a vehicle must be known. These are: (a) autopilot - air frame stability problem, and (b) the dynamic load problem. Of these two, the first one is considerably more important. To avoid excessive stability margins due to ignorance of structural characteristics or additional autopilot complexity, the dynamic properties of a structure must be known to a high degree of accuracy. For example, the permissible tolerance on the fundamental mode frequency may be as low as ±5 percent and on modal slope at gyro locations ±25 percent. On the other side, the dynamic load problems normally do not require extreme accuracy of modal representation because, for most cases, dynamic loads contribute only a small portion of total loading that acts on the air frame. Even for those cases where loading is predominantly dynamic, such as during the launch sequence, a reasonable change in modal representation does not constitute a significant change in loads.

Titan III in its C configuration consists of a liquid core and two strap-on solid rocket motors. These motors are connected to the core by means of forward and aft ties making the structure redundant in pitch and providing a coupling between the longitudinal and the yaw motion (Figure 1). The core itself consists of two conventional stages similar to those of Titan II and a new upper stage, called transtage. The tanks of the transtage are located side by side and are supported by trusses from a common ring frame (Figure 2). The tanks by themselves are of unequal size and weight producing coupling in various planes.

Analytical representation of such a structure is difficult, not so much from the conceptual point of view, but rather from the enormous bookkeeping point of view. The basic Titan structure is a standard skin stringer type. The solid rocket motors are of monocoque construction. The equations of motion for each body can be derived using standard energy approach idealizing the structure as an equivalent beam possessing both the bending and shear modulae. Because of a considerable slenderness ratio, the local mass moments of inertia do not have to be considered.

The difficulty arises in coupling the individual components together. Matrix notation is of utmost importance in keeping the bookkeeping straight. The derivation of equations of motion maintains the matrix notation from the very concept to the final equations. It is needless to say that a large core capacity digital computer is required for the solution of the problem.

The vibration test of the Titan III model accomplished a very important task. It had demonstrated that it is quite feasible to use analysis as a final design tool and that tolerances obtained from the model test can be applied to the design of the control system of the full scale prototype.

METHOD OF ANALYSIS

The material in this section has been developed by Mr. C. S. Bodley of the Martin Company to whom the authors are indebted for permission to use it.

Titan III configurations, as mentioned earlier, are symmetric only with respect to the x-y plane (Figure 3). There is near symmetry with respect to the x-z plane, but mass differences

Approved for Public Release

Contrails

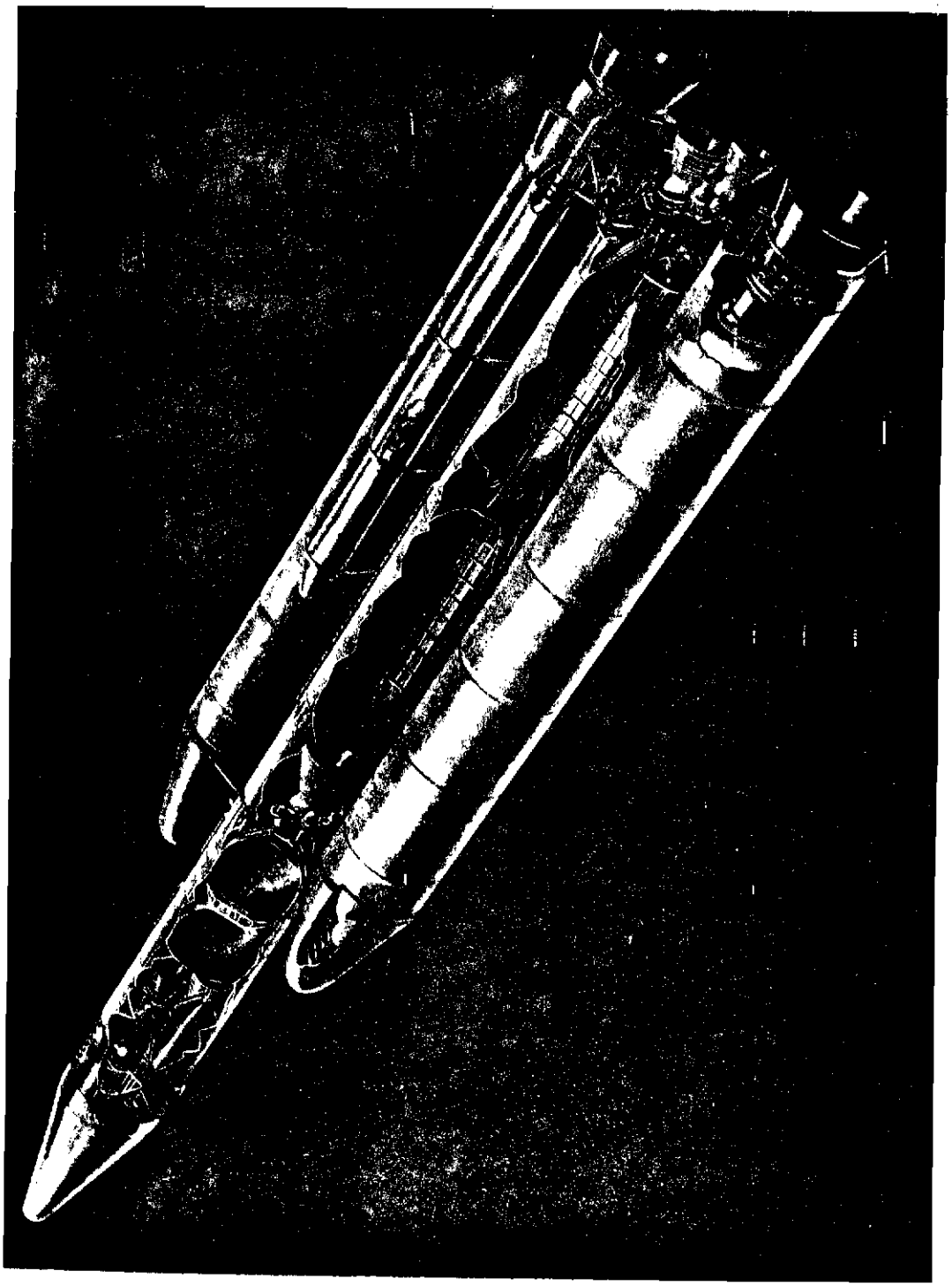

Figure 1.

Approved for Public Release

Contrails

Figure 2.

Approved for Public Release

Contrails

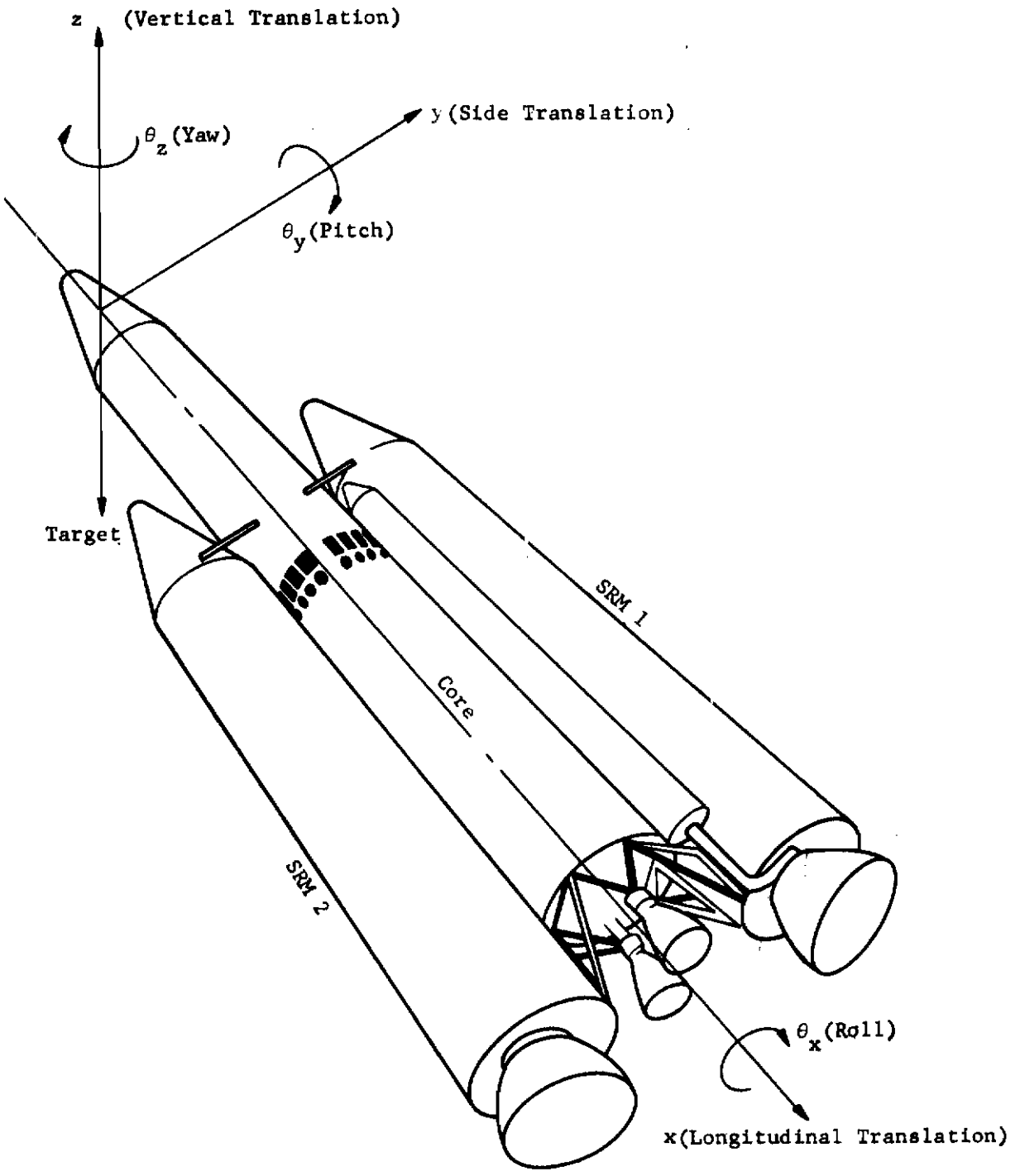

Figure 3. Vibration Analysis Sign Convention

Approved for Public Release

Contrails

in the transtage tanks destroy this. The x-y plane symmetry does significantly facilitate the analysis because yaw-longitudinal motion is uncoupled from pitch-torsion motion.

In performing the vibration analysis different types of generalized coordinates have been used to describe the equations of motion. In general, there are four types of generalized coordinates that can be used. They are defined herein as:

(1) discrete - relative

(2) discrete - absolute

(3) normal - relative

(4) normal - absolute

Any combination of the four types of coordinates can be used for a given analysis. In this analysis, the following types of coordinates have been selected:

TABLE I

LIST OF COMPONENTS AND COORDINATE TYPES

Component	Coordinate Type
Core shell bending (pitch & yaw)	discrete - absolute
Core shell longitudinal	discrete - absolute
Core shell torsion	discrete - absolute
Core tank bottoms and axial engines	discrete - absolute
Transtage tanks	normal - relative
Slosh	discrete - relative
Stage I, II and III Engine rotations	discrete - relative
Payload	normal - relative
SRM* bending, longitudinal and torsion	normal - absolute
*Solid Rocket Motors	

Tables 2 and 3 describe coordinate number assigned in the yaw-longitudinal and pitch-torsion plane analyses respectively.

Approved for Public Release

Contrails

TABLE II

LIST OF COORDINATES AND COORDINATE NUMBERS

FOR YAW PLANE

Coordinate No.	Coordinate Description
1-15	Translation of core (yaw)
16-30	Rotation of core
31-45	Translation of core (longitudinal)
46-51	Stage I engine, fuel and oxidizer tank bottoms
	Stage II engine, fuel and oxidizer tank bottoms
52, 53, 54	Transtage tank yaw-longitudinal modes
55, 56, 57	Stage I, II and III yaw engine rotations
58-63	Slosh modes
64-68	Payload yaw and longitudinal modes
69-80	SRM modes, yaw and longitudinal

TABLE III

LIST OF COORDINATES AND COORDINATE NUMBERS

FOR PITCH PLANE

Coordinate No.	Coordinate Description
1-15	Translation of Core (pitch)
16-30	Rotation of core
31-45	Rotation of core
46, 47, 48	Transtage tank pitch torsional modes
49-53	Step I, II and III pitch-roll engine rotations
54-59	Slosh modes
60-64	Payload pitch and torsional modes
65-76	SRM modes

Approved for Public Release

Contrails

Because of the complexity of the Titan III and because of the intent of this paper to describe the comparison of the theory with experiment, only a cursory symbolic treatment of the method of analysis is possible. To elucidate the basic philosophy of the analysis, only pitch analysis will be described. In addition, the transtage and slosh degrees of freedom shall be suppressed. Consequently, the following important items shall be described:

(a) Core stiffness matrix (b) Core mass matrix (c) Core to SRM coupling spring matrix (d) Payload stiffness and mass matrices

(1) Core stiffness matrix.

To generate stiffness coefficients for a flexural beam, consider an elemental segment which is loaded with a shear and moment at one end and restrained at the other end.

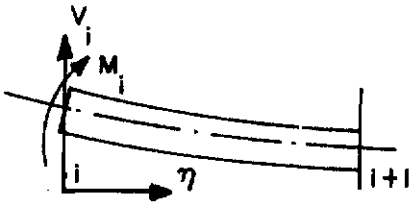

Figure 4. Element for Stiffness Coefficient Development

The strain energy for the i^{th} beam segment can be written as

$$U_i = \frac{1}{2}\begin{bmatrix} V_i & M_i \end{bmatrix}\begin{bmatrix} E_{11} & E_{12} \\ E_{21} & E_{22} \end{bmatrix}\begin{bmatrix} V_i \\ M_i \end{bmatrix} \tag{1}$$

where

$$E_{11} = \int_0^{\ell}\left(\frac{\eta^2}{EI} + \frac{1}{kAG}\right)d\eta$$

$$E_{12} = E_{21} = \int_0^{\ell}\frac{\eta\, d\eta}{EI}$$

$$E_{22} = \int_0^{\ell}\frac{d\eta}{EI}$$

Application of Castigliano's theorem results in the reciprocal strain energy expression

$$U_i = \frac{1}{2}\begin{bmatrix} \Delta\delta_i & \Delta\theta_i \end{bmatrix}\begin{bmatrix} k_{\delta\delta} & k_{\delta\theta} \\ k_{\theta\delta} & k_{\theta\theta} \end{bmatrix}\begin{bmatrix} \Delta\delta_i \\ \Delta\theta_i \end{bmatrix} \tag{2}$$

where the coefficients k_{ij} are computed by inversion of the energy matrix E_{ij} from Equation 1.

The coordinates $\Delta\delta_i$ and $\Delta\theta_i$ are deflections of point i relative to i + 1. The restraint at point i + 1 is removed by application of the transformation.

Approved for Public Release

Contrails

$$\begin{bmatrix} \Delta\delta_i \\ \Delta\theta_i \end{bmatrix} = \underbrace{\begin{bmatrix} 1 & -1 & 0 & -\ell_i \\ 0 & 0 & 1 & -1 \end{bmatrix}}_{[T_i]} \begin{bmatrix} \delta_i \\ \delta_{i+1} \\ \theta_i \\ \theta_{i+1} \end{bmatrix} \tag{3}$$

Substitution of Equation 3 into Equation 2 yield the energy expression in terms of absolute coordinates

$$U_i = \frac{1}{2} \begin{bmatrix} \delta_i & \delta_{i+1} & \theta_i & \theta_{i+1} \end{bmatrix} \begin{bmatrix} K_{ij} \end{bmatrix} \begin{bmatrix} \delta_i \\ \delta_{i+1} \\ \theta_i \\ \theta_{i+1} \end{bmatrix} \tag{4}$$

where

$$K_{ij} = T_i^T \, \mathbb{k}_{ij} \, T_i \tag{5}$$

Summation of strain energy contributions from all the segments yields a coupled stiffness matrix for the flexural beam which can be rearranged to have four partitions, each of tri-diagonal form

$$K = \begin{bmatrix} \times\times & & \times\times & \\ \times\times\times & & \times\times\times & \\ \times\times\times & & \times\times\times & \\ & \times\times & & \times\times \\ & \times\times\times & & \times\times\times \\ & \times\times\times & & \times\times\times \end{bmatrix} = \begin{bmatrix} K_{\delta\delta} & K_{\delta\theta} \\ K_{\theta\delta} & K_{\theta\theta} \end{bmatrix} \tag{6}$$

The 2 x 2 sub-partitions of this matrix are obtained by overlapping and adding common elements of beam segment sub-partitions.

Stiffness matrices for axially and torsionally loaded beam elements are of similar form.

(2) Beam Mass Matrix

Mass coefficients are generated by using a cubic interpolation formula. Consider a cubic function defined in the interval $x_i \leq x \leq x_{i+1}$. Assuming η to be a local coordinate

$$\delta(\eta) = a\eta^3 + b\eta^2 + c\eta + d \tag{7}$$

where $\delta(\eta)$ is a deflection at point η, and

$$\eta = x - x_i$$

Also, let $\ell = x_{i+1} - x_i$.

Approved for Public Release

Contrails

$\theta(\eta)$ is the slope at point η, so that

$$\theta(\eta) \equiv -\frac{\partial \delta(\eta)}{\partial x}$$

The deflections $\delta(\eta)$ and slopes $\theta(\eta)$ can be written as a combination of the coordinates $\delta_i, \delta_{i+1}, \theta_i$ and θ_{i+1} as follows:

$$\delta(\eta) = \begin{bmatrix} \eta^3 & \eta^2 & \eta & 1 \end{bmatrix} \begin{bmatrix} 2/\ell^3 & -2/\ell^3 & -1/\ell^2 & -1/\ell^2 \\ -3/\ell^2 & 3/\ell^2 & 2/\ell & 1/\ell \\ 0 & 0 & -1 & 0 \\ 1 & 0 & 0 & 0 \end{bmatrix} \begin{bmatrix} \delta_i \\ \delta_{i+1} \\ \theta_i \\ \theta_{i+1} \end{bmatrix} \tag{8}$$

A differentiation of this expression with respect to η yields the expression for slopes

$$-\theta(\eta) = \begin{bmatrix} 3\eta^2 & 2\eta & 1 & 0 \end{bmatrix} \mathbf{C} \begin{bmatrix} \delta_i \\ \delta_{i+1} \\ \theta_i \\ \theta_{i+1} \end{bmatrix} \tag{9}$$

where **C** is the kernel matrix of Equation 8.

The kinetic energy contribution of a beam segment can be defined in terms of coordinates η as follows

$$T = \frac{1}{2} \int_0^{\ell} \left(m(\eta)\, \dot{\delta}^2(\eta, t) + I(\eta)\, \dot{\theta}^2(\eta, t) \right) d\eta$$

or in the matrix form

$$T = \frac{1}{2} \int_0^{\ell} \begin{bmatrix} \dot{\delta}(\eta) & \dot{\theta}(\eta) \end{bmatrix} \begin{bmatrix} m(\eta) & 0 \\ 0 & I(\eta) \end{bmatrix} \begin{bmatrix} \dot{\delta}(\eta) \\ \dot{\theta}(\eta) \end{bmatrix} d\eta \tag{10}$$

The time dependency of derivatives is implied.

Substituting (9) into (10), the segment mass matrix can be defined as

$$\mathbf{M}_i = \mathbf{C}^T \left(\int_0^{\ell} \begin{bmatrix} \eta^6 & \eta^5 & \eta^4 & \eta^3 \\ \eta^5 & \eta^4 & \eta^3 & \eta^2 \\ \eta^4 & \eta^3 & \eta^2 & \eta^1 \\ \eta^3 & \eta^2 & \eta^1 & 1 \end{bmatrix} m(\eta)\, d\eta + \right.$$

$$\left. + \int_0^{\ell} \begin{bmatrix} 9\eta^4 & 6\eta^3 & 3\eta^2 & 0 \\ 6\eta^3 & 4\eta^2 & 2\eta & 0 \\ 3\eta^2 & 2\eta & 1 & 0 \\ 0 & 0 & 0 & 0 \end{bmatrix} I(\eta)\, d\eta \right) \mathbf{C} \tag{11}$$

Approved for Public Release

Contrails

This is a (4 x 4) matrix of mass coefficients which correspond to two translational and two rotational velocities. The (2 x 2) sub-partitions of segment mass matrix are overlapped and added to form the composite beam mass matrix which can be constructed with four partitions, each of tri-diagonal form, similar to the composite stiffness matrix. For a beam segment of uniform mass distribution and zero moment of inertia distribution, this mass is identical to Archer's consistent mass matrix (Reference 1) with the exception of sign convention.

Mass coefficients for torsional and axial beam segments are generated by assuring linear deflection functions.

(3) Core to SRM coupling spring Matrix

The attachment structure is considered in two parts: Forward linkage and Aft linkage. The forward linkage is comprised of a shear tie in the transverse (y) direction, a shear tie in the target (z) direction, and a torque tie. The aft linkage is comprised of shear ties in the three orthogonal directions (x, y, z), and moment ties with respect to x and y axes; there is rotational freedom with respect to the z-axis, (see Figure 5).

Flexibility influence coefficients are obtained for the fore and aft linkages with a complete (built-in) constraint at the core centerline. There are implied constraints at the SRM centerlines; these constraints are: Moment with respect to the z-axis for the aft linkage and force in the x direction, moment with respect to y and z axes for the forward linkage. These constraints are necessary in the generation of linkage flexibility influence coefficients for static stability. The influence coefficients are, of course, deflections at SRM centerlines due to unit generalized forces at SRM centerlines.

The strain energy contribution of the attachment linkages may be expressed in terms of the flexibility influence coefficients and the generalized forces acting at the SRM centerlines. Application of Castigliano's theorem allows for the reciprocal strain energy expression which involves linkage stiffness influence coefficients and elastic deflections "across the linkages".

These elastic deflections reflect the aforementioned constraints.

In order to "tie" the core and SRM's together with the linkage stiffness coefficients the constraints must be relieved. This is accomplished by equations of the form:

$$\begin{aligned} \Delta\vec{\delta}_i &= \vec{\delta}_i - (\vec{\delta}_{ref} + \vec{\theta}_{ref} \times \vec{r}) \\ \Delta\vec{\theta}_i &= \vec{\theta}_i - \vec{\theta}_{ref} \end{aligned} \tag{12}$$

where $\vec{\delta}_{ref}$ and $\vec{\theta}_{ref}$ are absolute generalized deflections corresponding to the points of constraint, $\vec{\delta}_i, \vec{\theta}_i$ and $\Delta\vec{\delta}_i, \Delta\vec{\theta}_i$ are respectively the absolute and elastic generalized deflections at point (i), and $\vec{r}$ is a vector directed from the constraint point to point (i).

Since normal absolute corrdinates are selected to represent SRM motion, transformations relating the components of $\vec{\delta}_i$ and $\vec{\theta}_i$ to the SRM normal coordinates $\xi^{(j)}$ are made.

Finally, the elastic deflections "across the linkage" are expressed in terms of discrete absolute deflections of the core centerline points and normal absolute deflections of the core centerline points and normal absolute deflections of the SRM's, thus affecting generation of the linkage stiffness coefficients.

(4) Payload Stiffness and Mass Matrices

Payload motion is represented by normal-relative coordinates. Payload modal deflections and frequencies are obtained for the payload contilevered at the payload-core interface. The

Approved for Public Release

Contrails

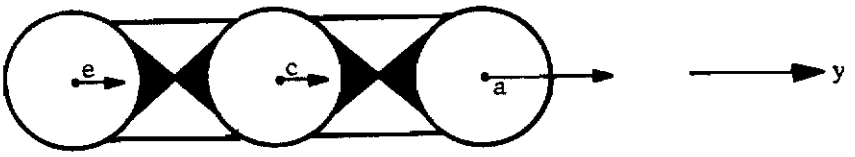

Forward-Linkage Configuration (Yaw Plane)

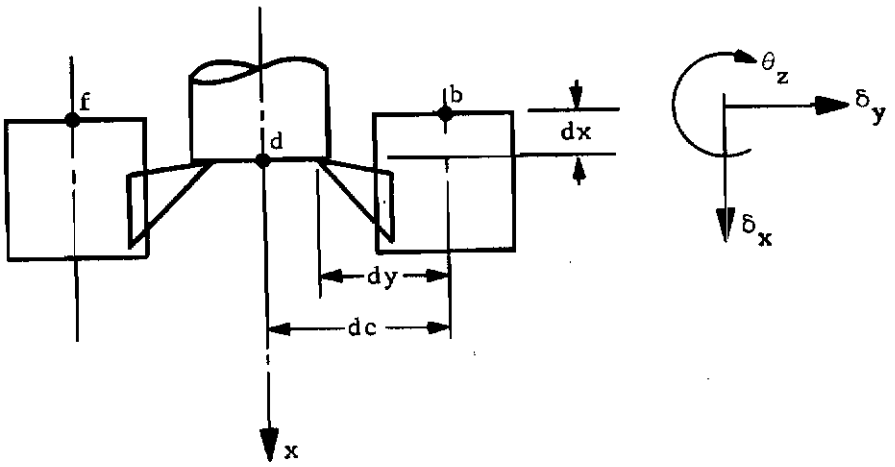

Figure 5. Aft-Linkage Configuration (Yaw Plane)

Approved for Public Release

Contrails

absolute motion of the payload is then expressed as a superposition of discrete absolute motion of the payload interface and the cantilevered payload normal modes. Symbolically, this is

$$q_{payload} = \left[T_P \;\vdots\; \phi_{payload} \right] \begin{bmatrix} q_{core} \\ \xi_{payload} \end{bmatrix} \tag{13}$$

where T is a simple geometric transformation.

The kinetic energy contribution of the payload is

$$T_{payload} = \frac{1}{2} \left[\dot{q}^T_{core} \; \dot{\xi}^T_{payload} \right] \underbrace{\begin{bmatrix} T_p^T \\ \phi_{payload} \end{bmatrix} M_{payload} \left[T_p \; \phi_{payload} \right]}_{\bar{M}_{payload}} \begin{bmatrix} \dot{q}_{core} \\ \dot{\xi}_{payload} \end{bmatrix} \tag{14}$$

where

$M_{payload}$ and $\bar{M}_{payload}$ are

original and final payload mass matrices respectively.

The choice of normal relative coordinates for the payload implies inertial coupling, but no stiffness coupling. The final payload stiffness matrix has only diagonal elements of the form $\left[M_{aq}\, \omega^2 \right]$ corresponding to the coordinates ξ where $\left(M_{eq}\, \omega^2 \right)_j$ is the generalized stiffness in the jth cantilevered payload mode.

The final composite stiffness and mass matrices are obtained by summing all the component matrices with each component matrix expanded to correspond to the final coordinates.

The eigenvectors and eigenvalues of the system are extracted by using the serial Jacobi method of successive rotations.

EXPERIMENTAL TECHNIQUE

Experimental verification of the vibration analyses can be accomplished by performing a vibration test on a full scale article or on a dynamically similar model. The important advantage of a full scale testing lies, obviously, in the accuracy of simulation. However, this simulation consists only of hardware simulation. Environment simulation is difficult, if not impossible, to achieve. First, there is a problem of suspending the vehicle in such a way as to separate sufficiently the suspension modes from the elastic modes. The larger the missile, the more difficult is the task. The second problem arises from the fact that only "1 g" field can be simulated during the test. If any skin buckling due to flight loads should occur, this will not happen during the vibration test. Also, the slosh frequencies are incorrect because they depend on the acceleration. The last technical problem is the difficulty in obtaining and handling a large quantity of inert propellant of proper density. In addition to factors mentioned, economic factors and schedules are of significance.

Considering now the problems with model testing, it appears that most of the positive factors listed for full scale vibration testing become negative and, vice versa, the negative factors become positive. Schedules are no longer a significant problem because the model can be built concurrently with the full scale article. Cost is considerably lower. Handling and set up problems are insignificant. The only question is how truly can one simulate the full scale

Approved for Public Release

Contrails

structure. In case of Titan III, a 20 percent factor was selected because it was felt that this size is large enough to facilitate exact duplication of the full scale structure yet small enough not to present a problem in handling and testing.

Figure 6 shows the erected model as the test facility at NASA, Langley Field. The test was performed for a number of payload weights and propellant conditions.

Three basic items obtained from these tests were: (1) natural frequencies, (2) modal displacements and (3) damping ratios. Modal slopes were obtained by differentiation of the displacement curves. To illustrate the consistency of analytical and experimental data, several forms of comparisons were developed and are presented below. The damping ratios, of course, cannot be estimated analytically and, therefore, no comparison is attempted. Orthogonality of the experimental modes was excellent for most cases.

Before an actual comparison is presented, it must be remembered that model simulation of the full scale article was not completely perfect. Slight deviations in the type of construction such as shapes of stringers made the model structure somewhat less stiff in certain areas. This is demonstrated in Figure 7. The mass simulation was excellent with practically no deviation from the full scale article.

A graphical comparison of analytical mode shapes of the full scale article and of the model with those obtained experimentally is shown in Figure 8 through 19. In most cases, the experimental data are closer to model analysis. Frequencies do not exhibit a definite trend.

To express the tolerances of frequencies, slopes and modal deflections at various gyro stations numerically, a statistical tolerance study was performed. The data is categorized by various groups.

The grouping was done according to payload weight, pitch or yaw condition, time of flight and gyro station. In addition, in each group the data was subgrouped according to mode. By sorting data into groups, statistical testing by an analysis of variance was accomplished to determine whether or not one of the factors has a significant effect over the other factors. A transformation of the model data to full scale normalized data indicated a trend toward normal distribution. The results of this tolerance study are presented in Table 4.

The data is given in percent of the corresponding nominal value at the tip station. The slope and deflection tolerances are given in terms of standard deviations. Frequency tolerances are given in a summary form for 99% confidence level in Table 5.

CONCLUSIONS

The highlights of a fairly extensive tolerance study shown here indicate that it is feasible to assume that the vibration analysis of a reasonably complex structure such as Titan III provides accuracy which is, for most cases, sufficient for the design of the control system. Although this is true in a statistical sense, deviations for specific configurations may be large enough so that a verification test is required. If a test is desirable, a model should be considered as an economical means of obtaining the confirmation of analyses.

Approved for Public Release

Contrails

TABLE IV

MODAL DISPLACEMENT AND SLOPE STANDARD DEVIATIONS

ϕ = Modal displacement, θ = Modal slope

Description of group		Values of tolerances in %		
		Mode 1	Mode 2	Mode 3
All payloads, all flight times pitch and yaw planes	ϕ θ	6 36	21 50	28 45
All payloads, all flight times pitch plane	ϕ θ	7 47	12 20	13 12
All payloads, all flight times yaw plane	ϕ θ	6 25	29 99	121 141
5,000 lb payload, all flight times pitch and yaw planes	ϕ θ	3 21	10 37	9 36
26,000 lb payload, all flight times pitch and yaw planes	ϕ θ	7 48	51 31	356 39
45,000 lb payload, all flight times pitch and yaw planes	ϕ θ	11 54	50 147	227 37
All payloads, flight time = 0 sec. pitch and yaw planes	ϕ θ	8 35	34 47	19 80
All payloads, flight time = 53 sec. pitch and yaw planes	ϕ θ	7 25	18 46	20 17
All payloads, flight time = 105 sec. pitch and yaw planes	ϕ θ	2 38	14 35	36 10

TABLE V

MODAL FREQUENCY TOLERANCES, 26,000-POUND PAYLOAD

Plane	Time of flight sec.	Mode 1 %	Mode 2 %	Mode 3 %
Pitch	0	1.62 ± 3.6	2.75 ± 7.3	5.08 ± 14.7
Pitch	105	1.90 ± 3.1	3.76 ± 5.3	7.05 ± 10.6
Yaw	0	1.44 ± 4	2.65 ± 7.5	3.94 ± 19
Yaw	105	1.74 ± 3.4	3.57 ± 5.6	5.75 ± 13

The tolerances are for 99 percent confidence level

Approved for Public Release

Contrails

Figure 6. Erosion Mo[illegible]

Approved for Public Release

Contrails

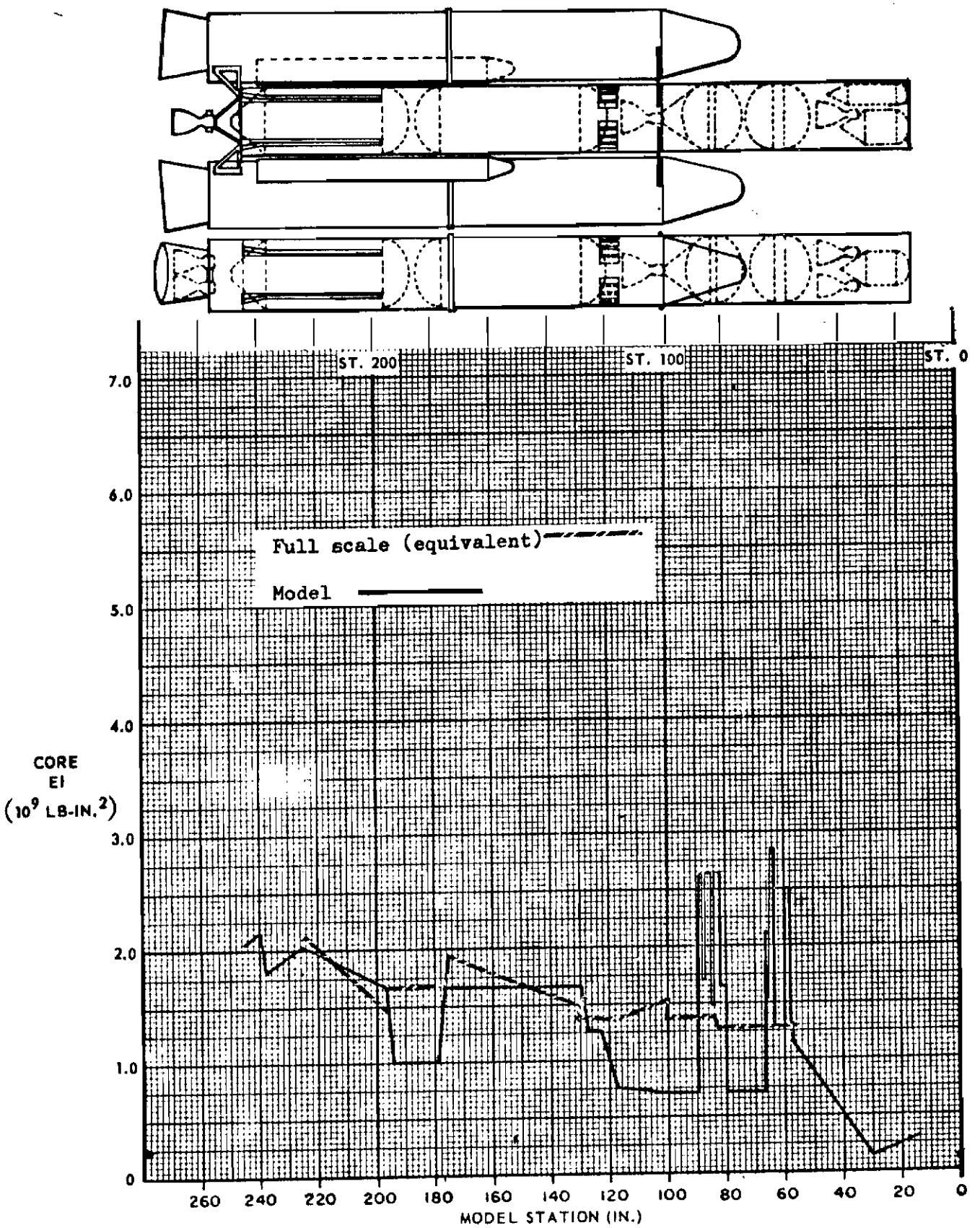

Figure 7. Stiffness Data

Approved for Public Release

Contrails

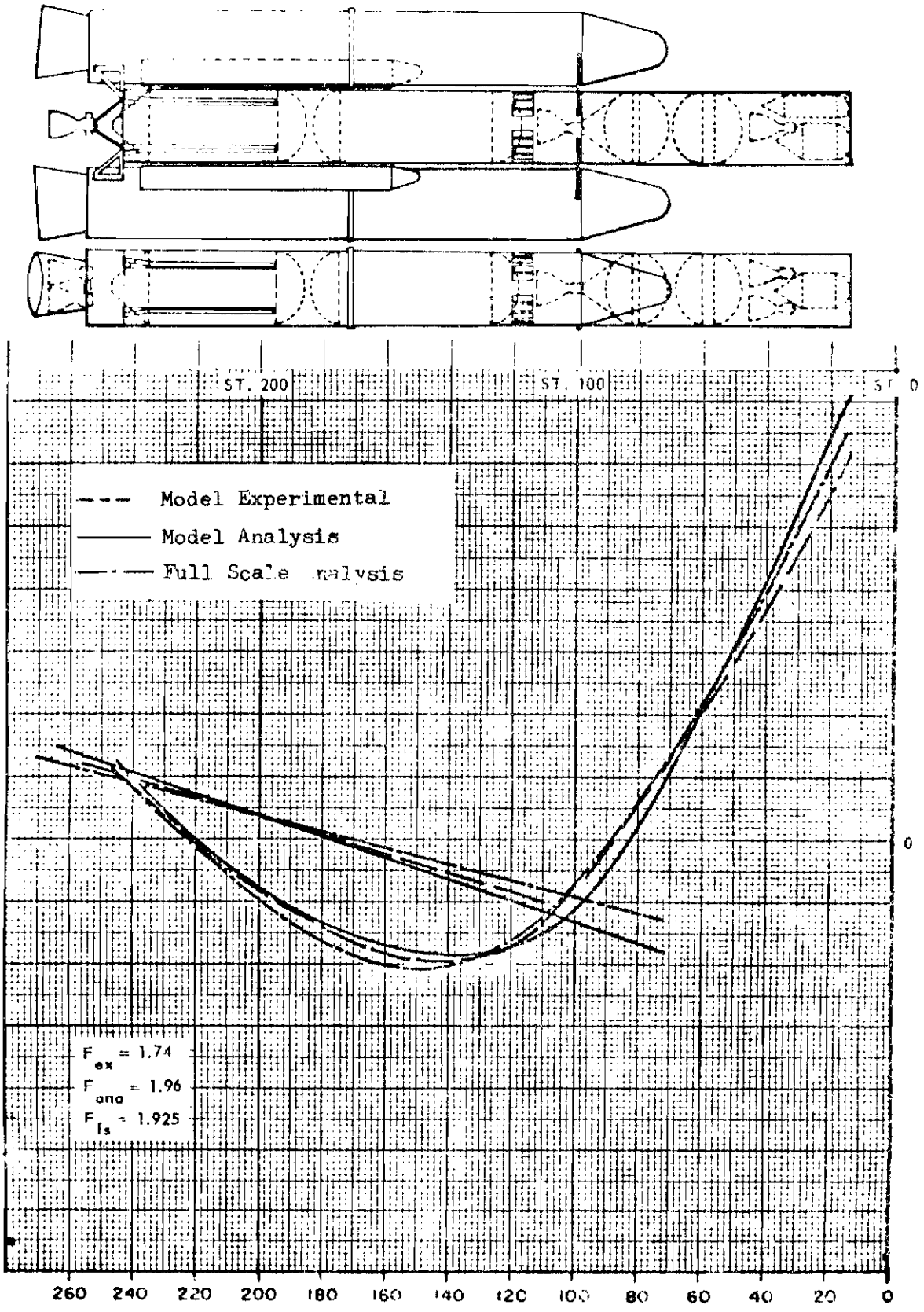

Figure 8. Configuration C - Pitch Payload 5000 Lb [illegible] Sec

Approved for Public Release

Contrails

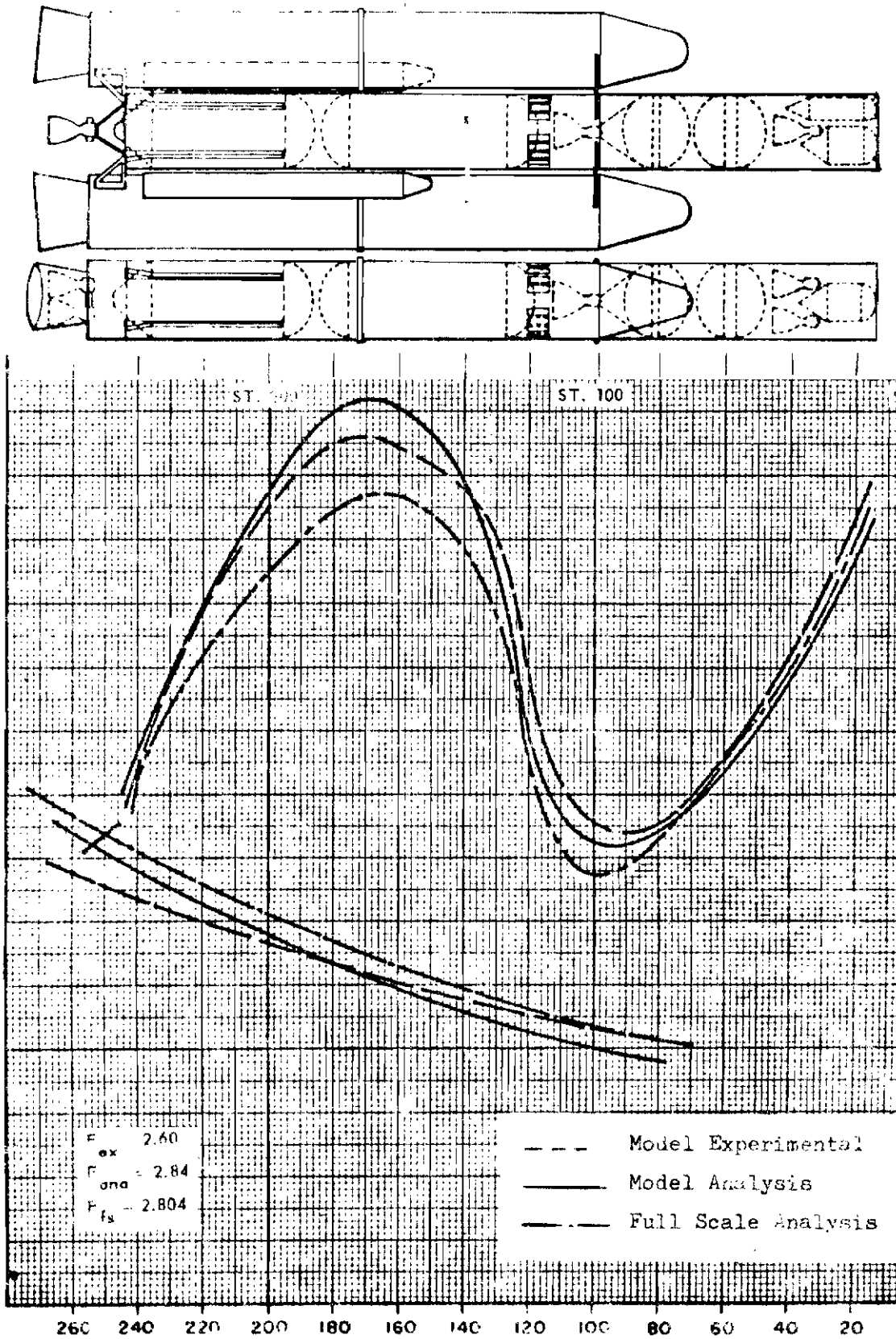

Figure 9 Configeration C - Pitch Payload 5000 Lb T = 0 Sec
MODE 2

Approved for Public Release

Contrails

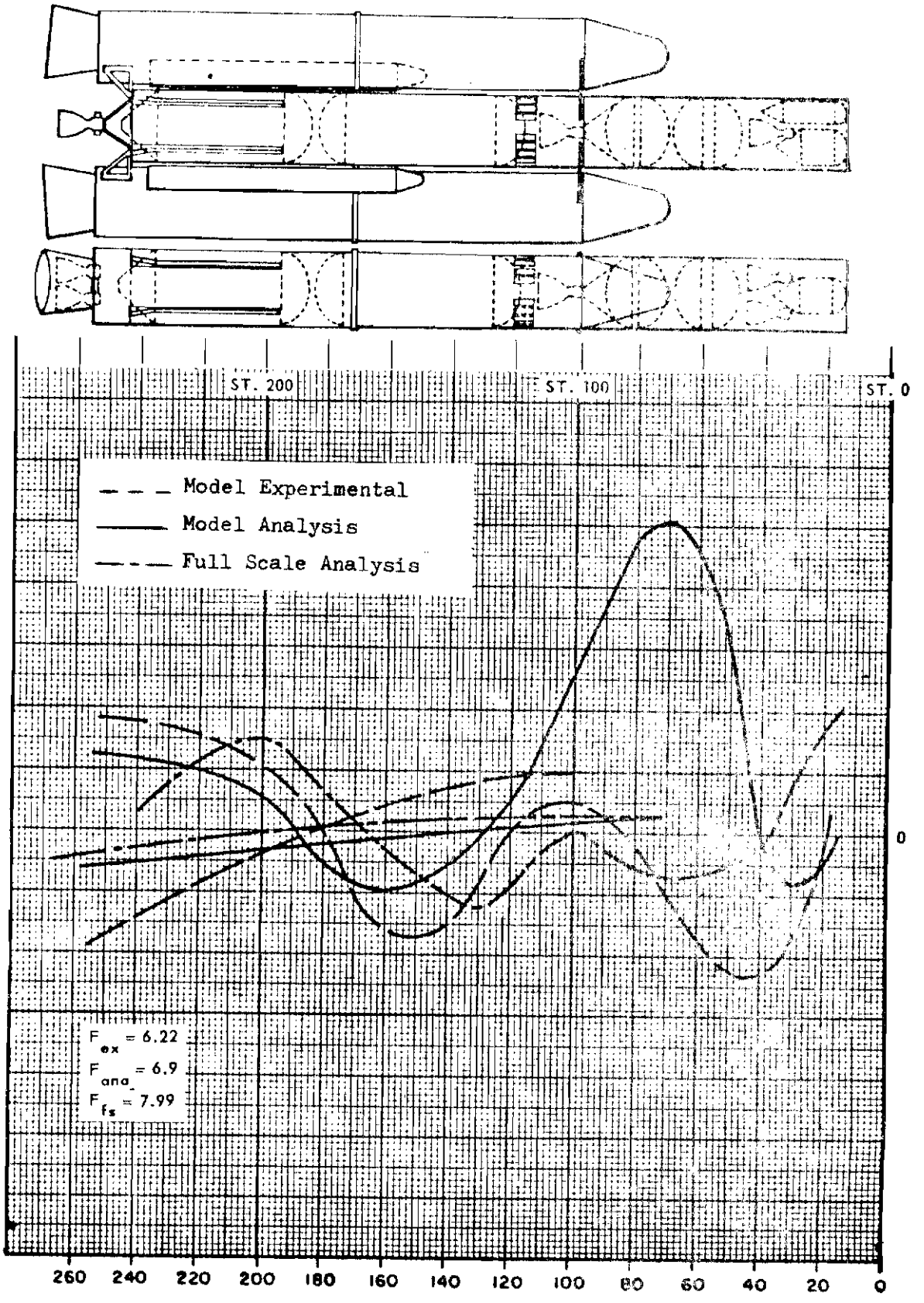

Figure 10. Configuration C - Pitch Payload 5000 Lb T - 0 Sec
MODE 3

Approved for Public Release

Contrails

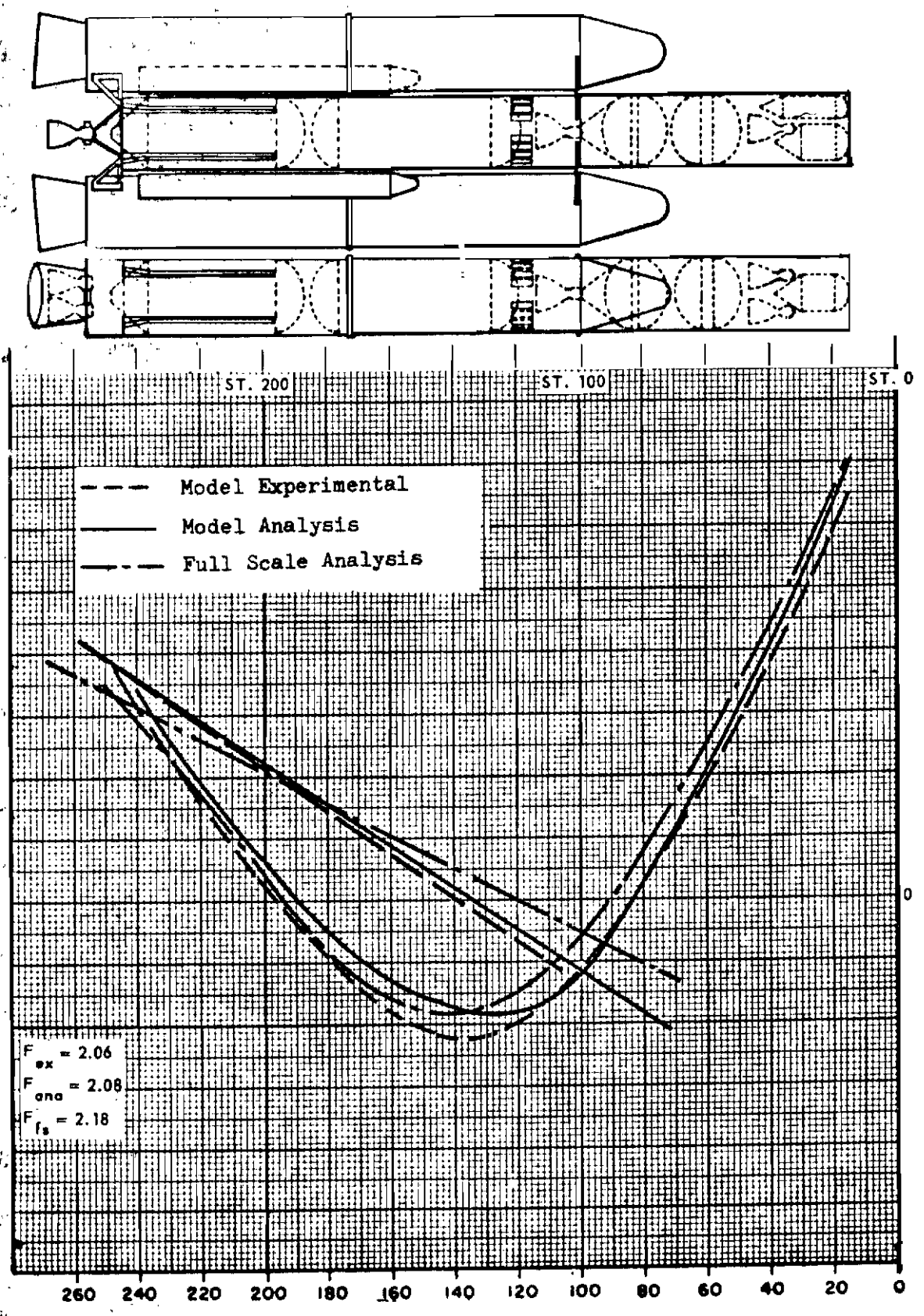

Figure 11. Configuration C - Pitch Payload 5000 Lb T = 105 Sec
MODE 1

Approved for Public Release

Contrails

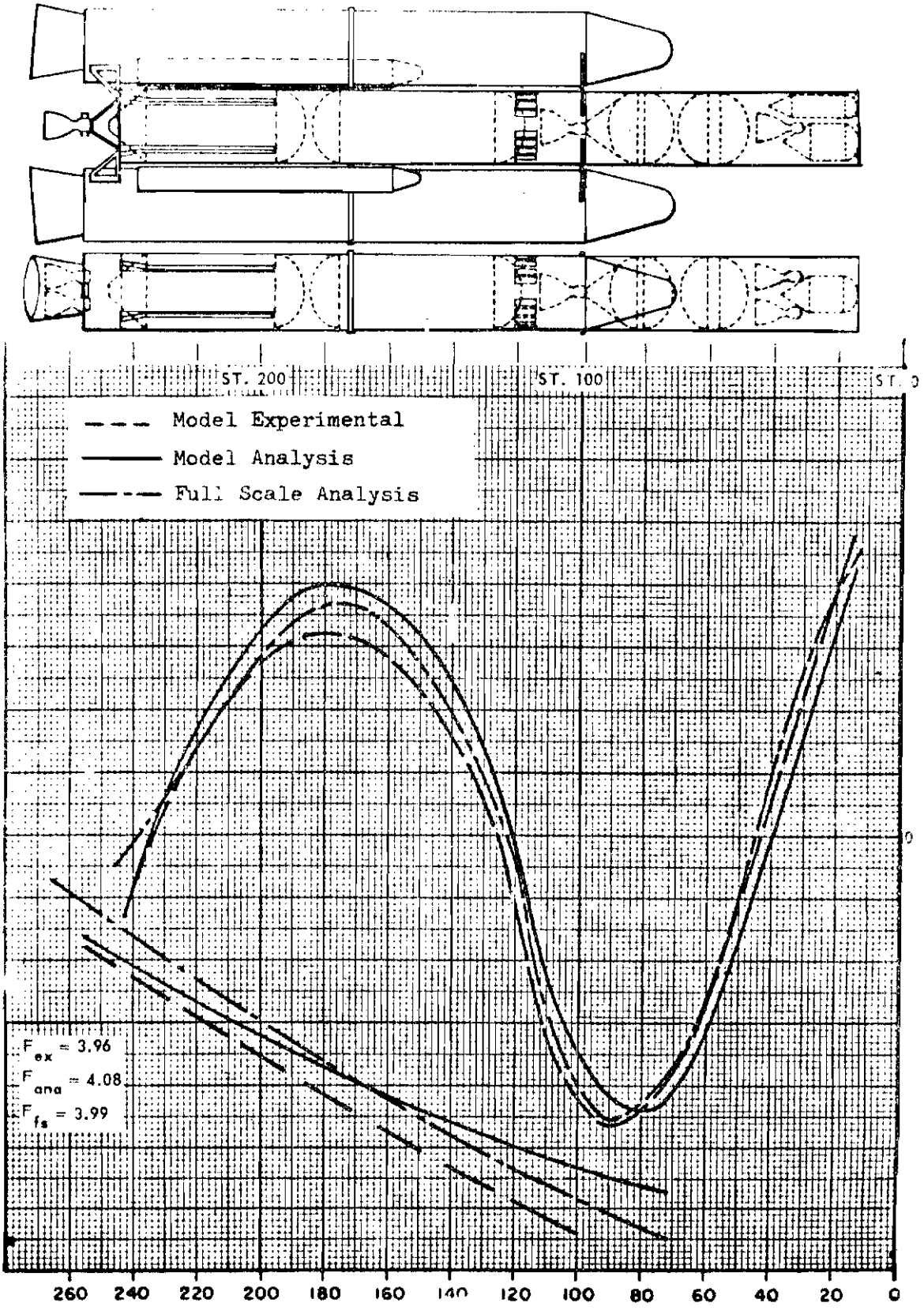

Figure 12. Configuration C - Pitch Payload 5000 Lb T = 105 Sec
MODE 2

Approved for Public Release

Contrails

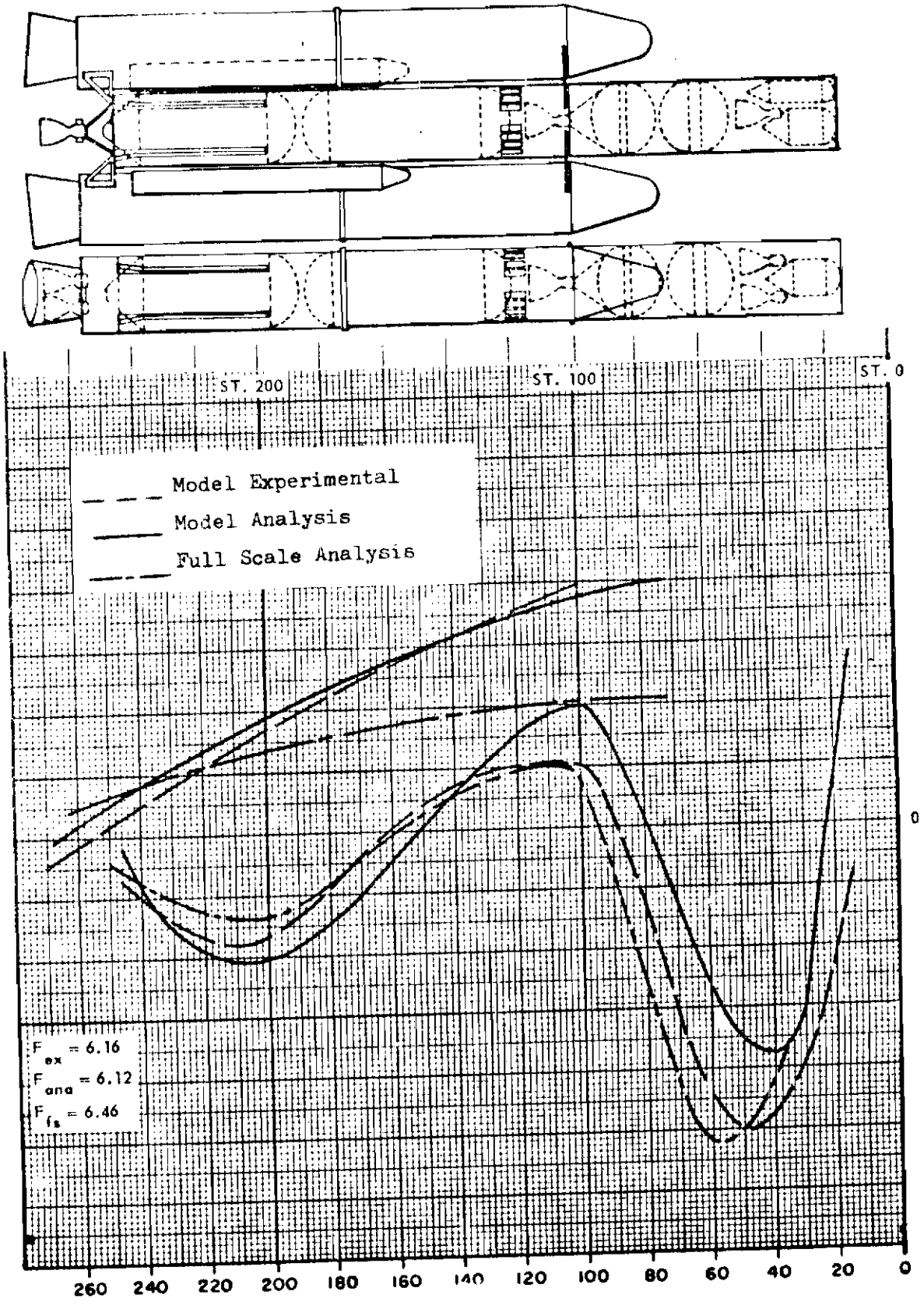

Figure 13. Configuration C - Pitch Payload 5000 Lb T = 105 Sec MODE 3

Approved for Public Release

Contrails

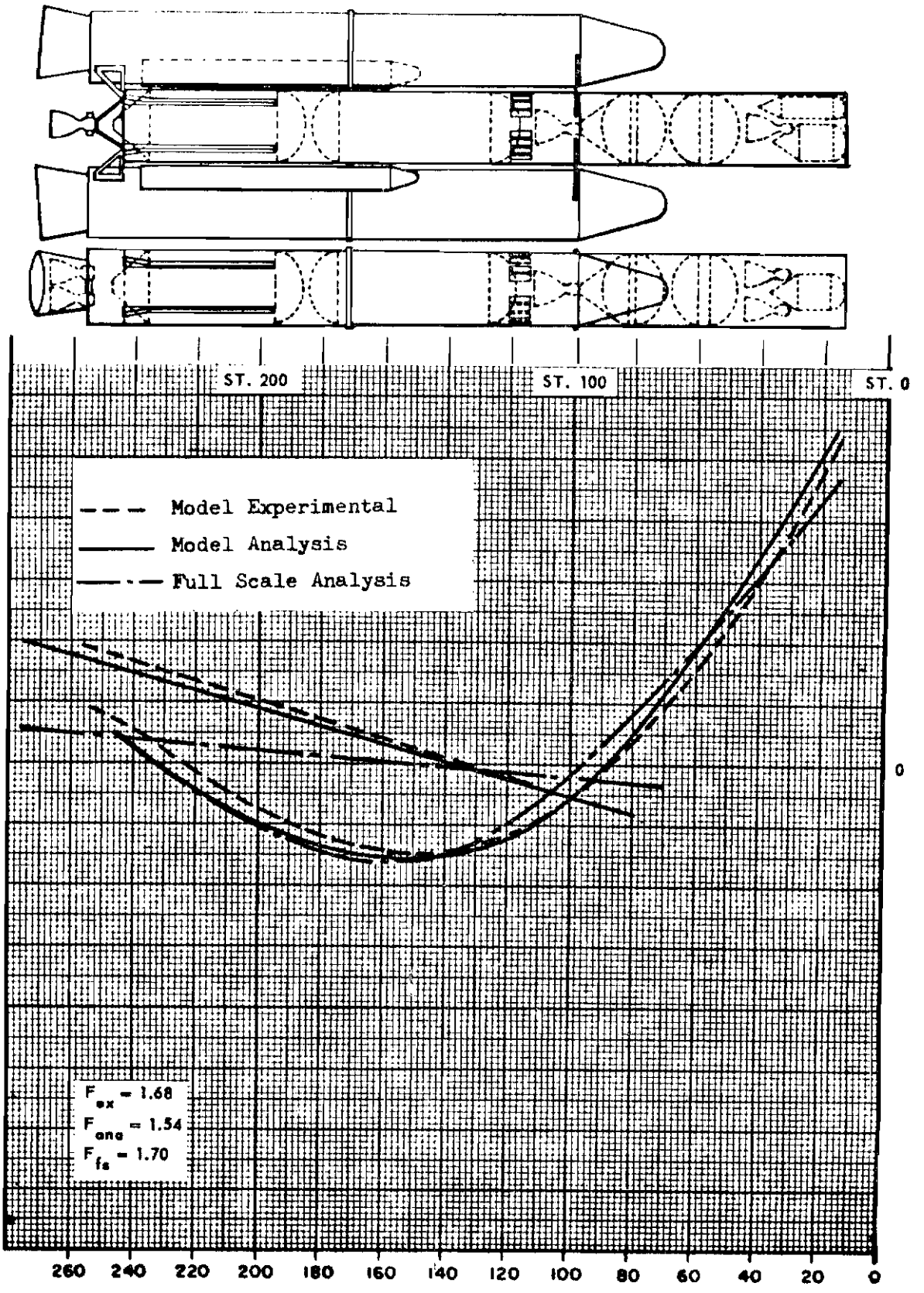

Figure 14. Configuration C - YAW Payload 5000 Lb T = 0 Sec
MODE 1

Approved for Public Release

Contrails

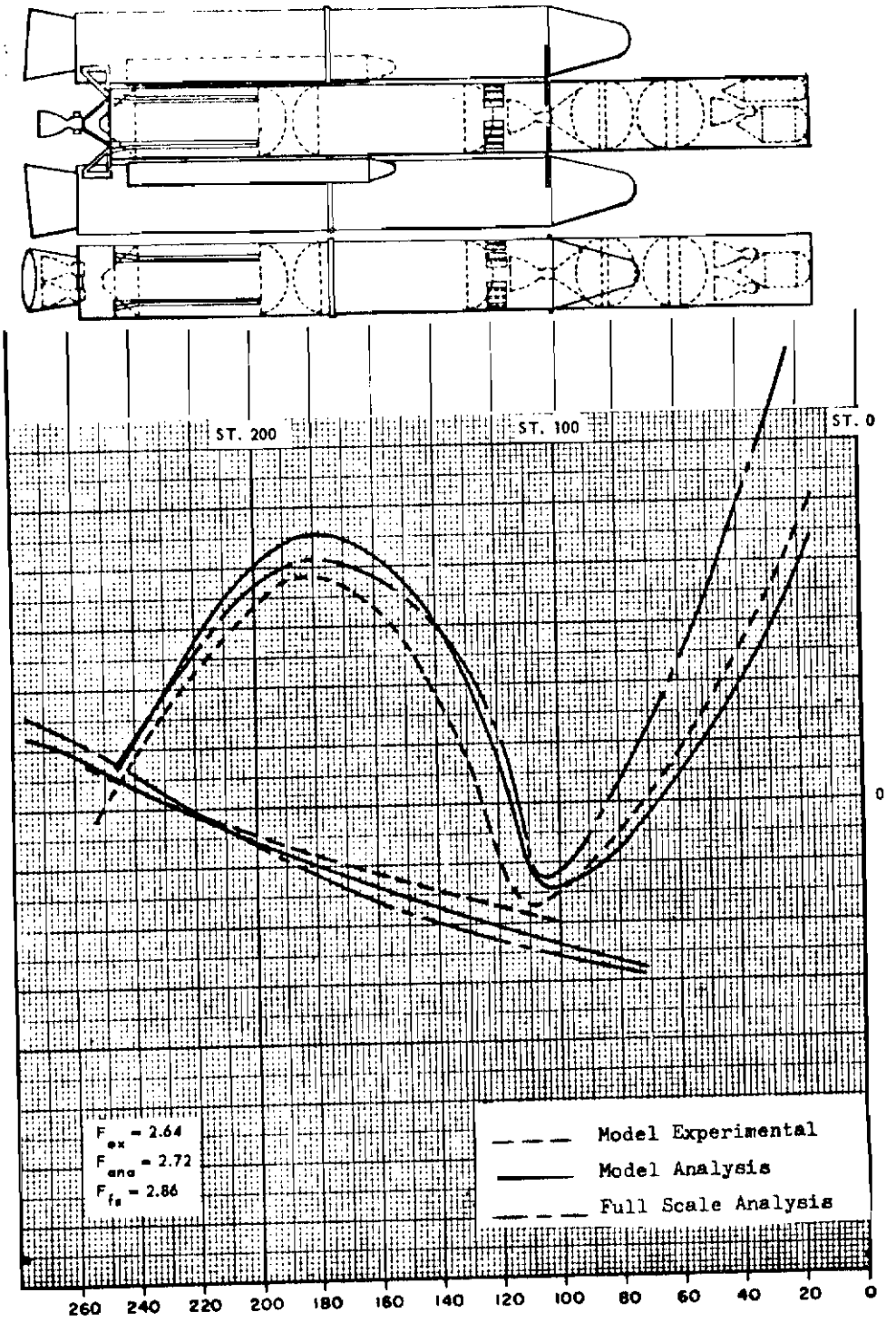

Figure 15. Configuration C - YAW Payload 5000 Lb T = 0 Sec
MODE 2

Approved for Public Release

Contrails

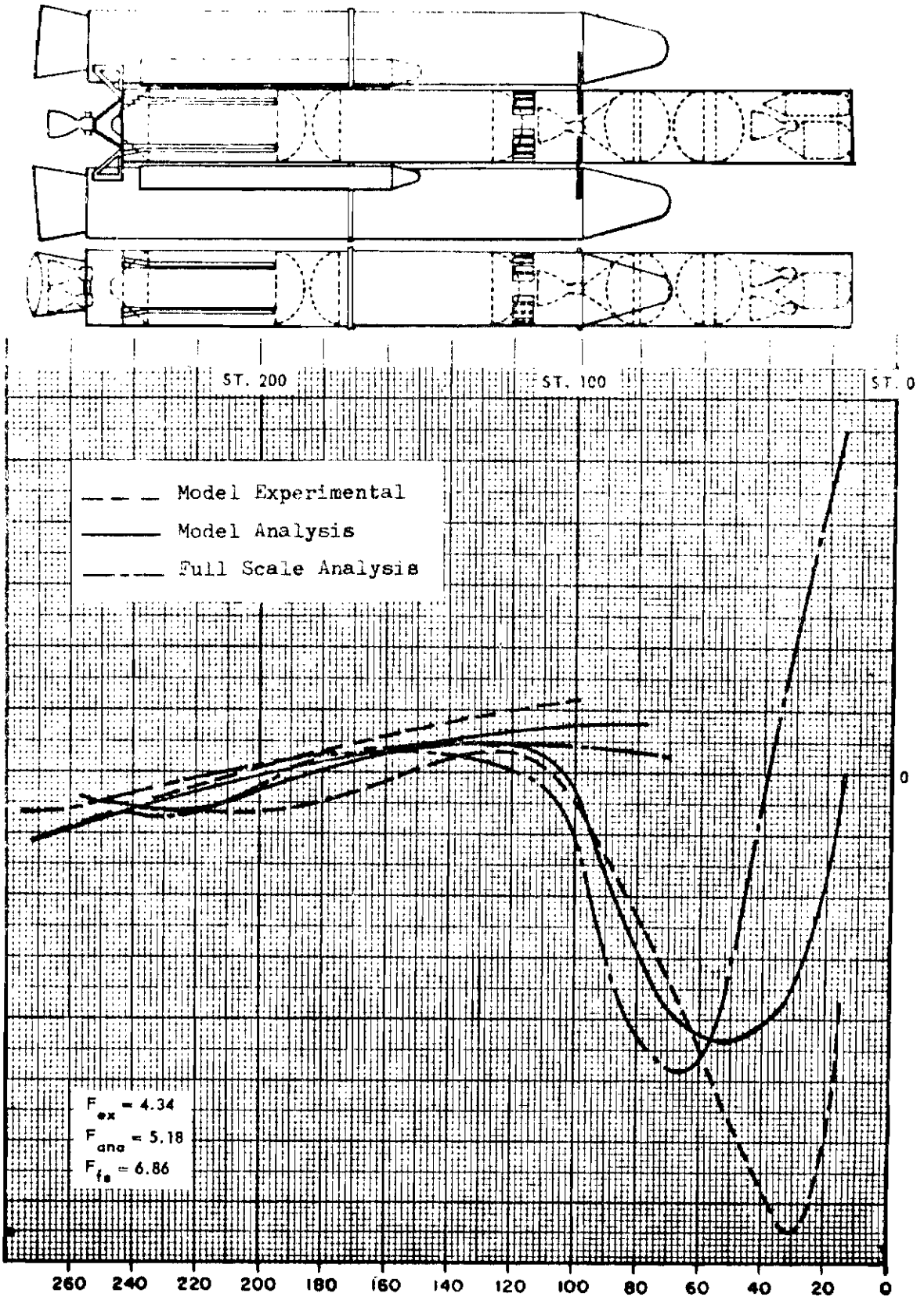

Figure 16. Configuration C - YAW Payload 5000 Lb T = 0 Sec
MODE 3

Approved for Public Release

Contrails

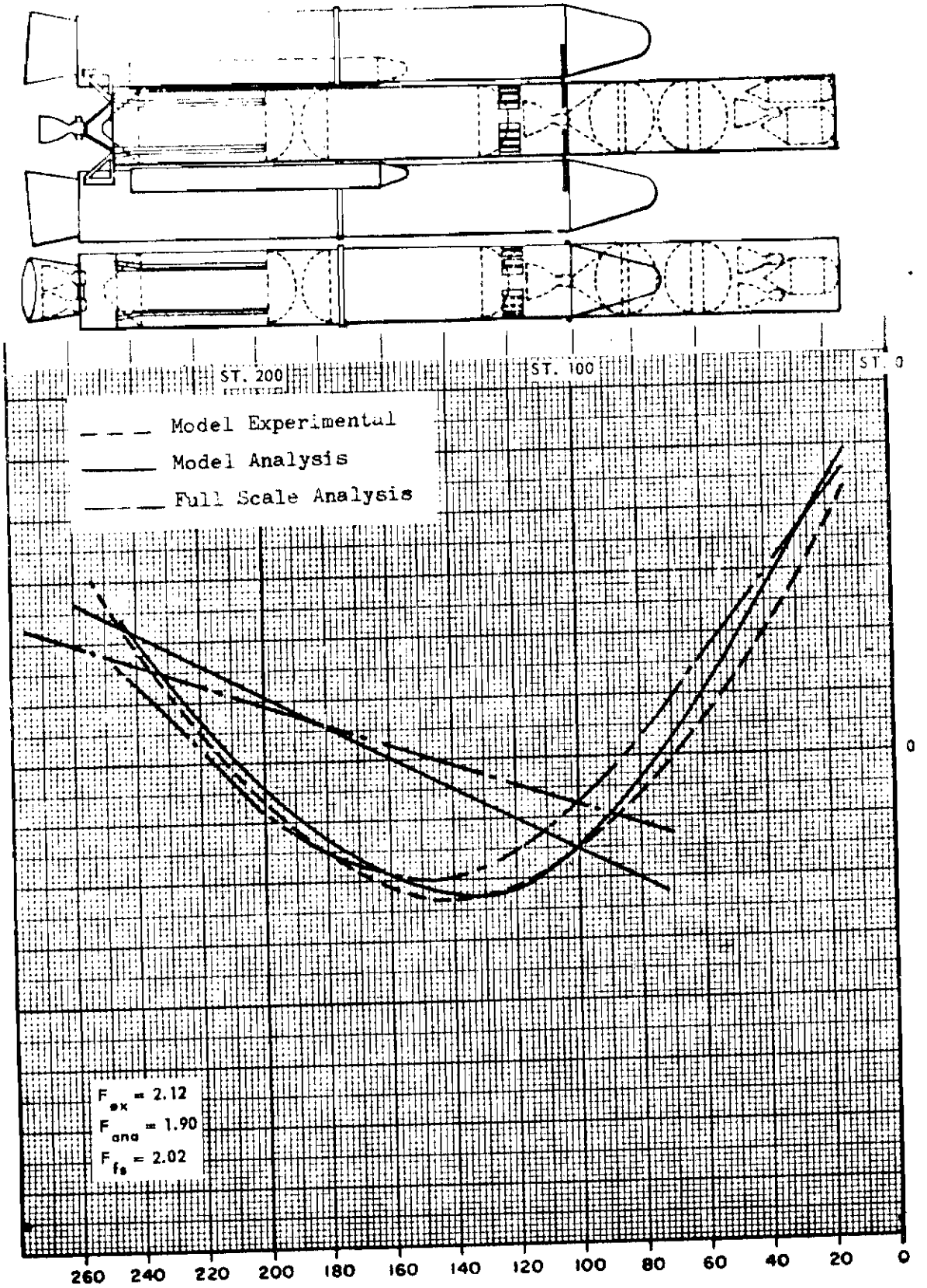

Figure 17. Configuration C - YAW Payload 5000 Lb T = 105 Sec
MODE 1

Approved for Public Release

Contrails

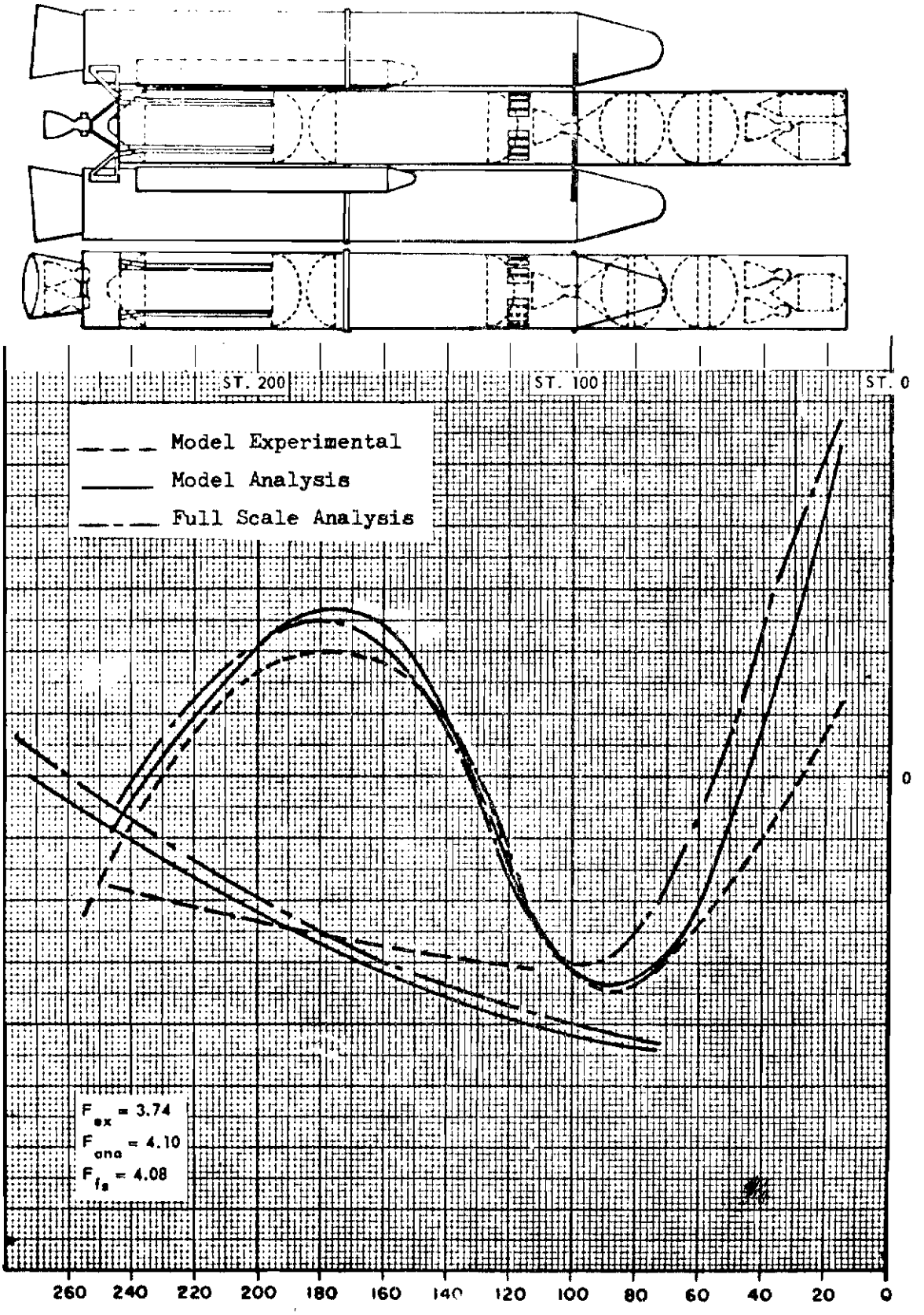

Figure 18. Configuration C - YAW Payload 5000 Lb T = 105 Sec
MODE 2

Approved for Public Release

Contrails

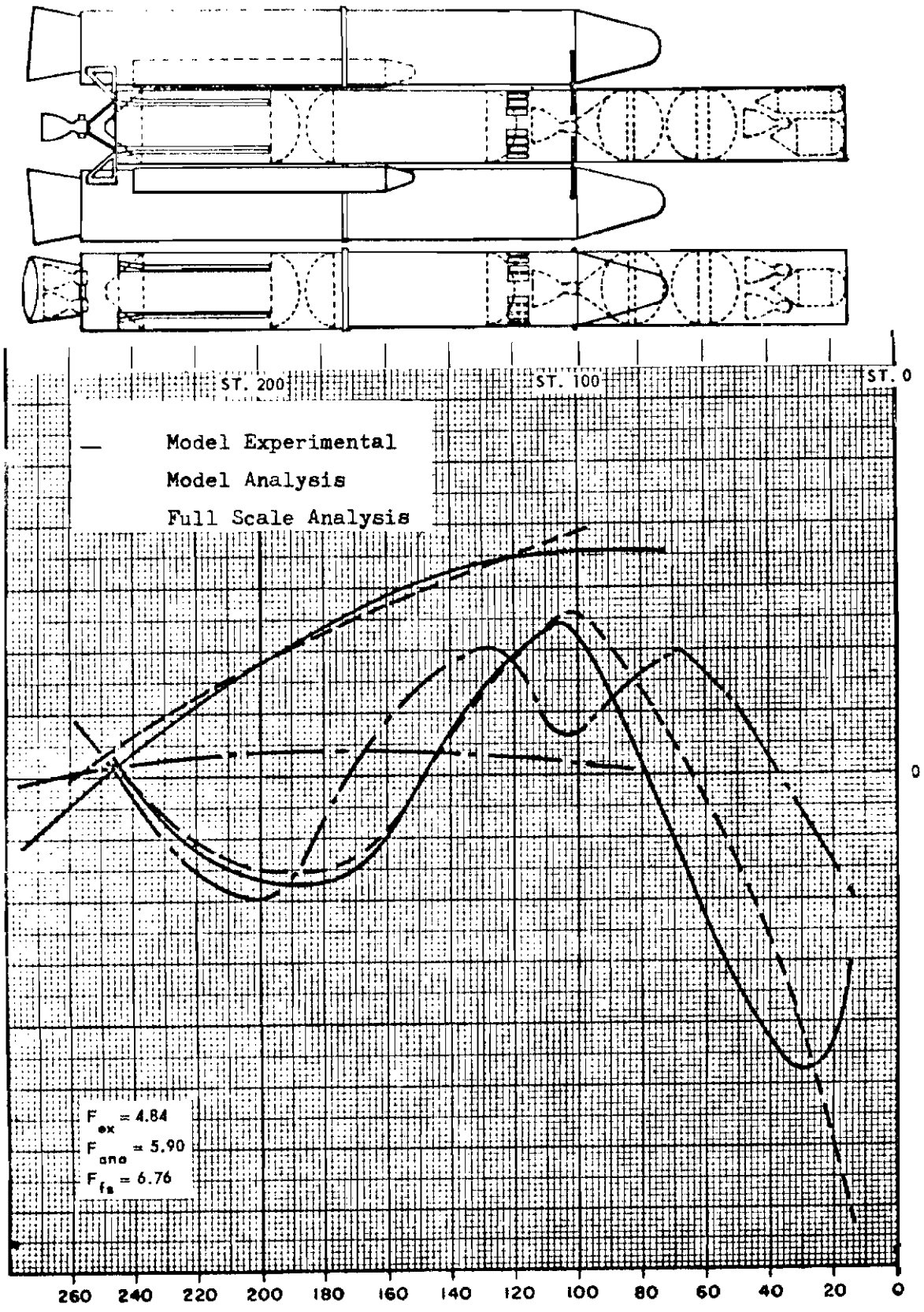

Figure 19. Configuration C - YAW Payload 5000 Lb T = 105 Sec
MODE 3

Approved for Public Release